Insights into the etiology and physiopathology of MODY5 / HNF1B pancreatic phenotype with a mouse model of the human disease

Evans Quilichini, Mélanie Fabre, Christoffer Nord, Thassadite Dirami, Axelle
Le Marec, Silvia Cereghini, Raymond C Pasek, Maureen Gannon, Ulf
Ahlgren, Cécile Haumaitre

▶ To cite this version:

ORIGINAL PAPER

Insights into the etiology and physiopathology of MODY5/HNF1B pancreatic phenotype with a mouse model of the human disease

Evans Quilichini[1†], Mélanie Fabre[1†], Christoffer Nord[3], Thassadite Dirami[1,2], Axelle Le Marec[1,2], Silvia Cereghini[1,2], Raymond C Pasek[4], Maureen Gannon[4], Ulf Ahlgren[3] and Cécile Haumaitre[1,2*]

[1] Centre National de la Recherche Scientifique (CNRS), UMR7622, Institut de Biologie Paris-Seine (IBPS), Paris, France
[2] Sorbonne Université, UMR7622-IBPS, Paris, France
[3] Umeå Centre for Molecular Medicine, Umeå University, Umeå, Sweden
[4] Department of Medicine, Vanderbilt University Medical Center, Nashville, TN, USA

*Correspondence to: C Haumaitre, CNRS UMR7622, Sorbonne Université, IBPS, 9 Quai Saint-Bernard, 75005 Paris, France.
E-mail: cecile.haumaitre@inserm.fr

[†]These authors contributed equally to this work.

Abstract

Maturity-onset diabetes of the young type 5 (MODY5) is due to heterozygous mutations or deletion of *HNF1B*. No mouse models are currently available to recapitulate the human MODY5 disease. Here, we investigate the pancreatic phenotype of a unique MODY5 mouse model generated by heterozygous insertion of a human *HNF1B* splicing mutation at the intron-2 splice donor site in the mouse genome. This *Hnf1b^{sp2/+}* model generated with targeted mutation of *Hnf1b* mimicking the c.544+1G>T (<IVS2nt+1G>T) mutation identified in humans, results in alternative transcripts and a 38% decrease of native *Hnf1b* transcript levels. As a clinical feature of MODY5 patients, the hypomorphic mouse model *Hnf1b^{sp2/+}* displays glucose intolerance. Whereas *Hnf1b^{sp2/+}* isolated islets showed no altered insulin secretion, we found a 65% decrease in pancreatic insulin content associated with a 30% decrease in total large islet volume and a 20% decrease in total β-cell volume. These defects were associated with a 30% decrease in expression of the pro-endocrine gene *Neurog3* that we previously identified as a direct target of Hnf1b, showing a developmental etiology. As another clinical feature of MODY5 patients, the *Hnf1b^{sp2/+}* pancreases display exocrine dysfunction with hypoplasia. We observed chronic pancreatitis with loss of acinar cells, acinar-to-ductal metaplasia, and lipomatosis, with upregulation of signaling pathways and impaired acinar cell regeneration. This was associated with ductal cell deficiency characterized by shortened primary cilia. Importantly, the *Hnf1b^{sp2/+}* mouse model reproduces the pancreatic features of the human MODY5/HNF1B disease, providing a unique *in vivo* tool for molecular studies of the endocrine and exocrine defects and to advance basic and translational research.

© 2021 The Authors. *The Journal of Pathology* published by John Wiley & Sons, Ltd. on behalf of The Pathological Society of Great Britain and Ireland.

Introduction

MODY (maturity-onset diabetes of the young) defines a dominantly inherited form of diabetes mellitus characterized by fasting hyperglycemia and diagnosed in children or young adults [1,2]. MODY results from heterozygous defects in 14 single genes affecting pancreatic islet function. This monogenic form of diabetes accounts for at least 1% of cases of diabetes mellitus. However, it is often misdiagnosed as type 1 (T1D) or type 2 diabetes (T2D), due to similarities in clinical presentation, and patients may receive inappropriate treatment [3–6]. The four most common causes of MODY are mutations in *HNF1A* (MODY3) (30–50%), *GCK* (MODY2) (30–50%), *HNF4A* (MODY1) (10%), and *HNF1B* (MODY5) (5%) [7,8].

HNF1B is a transcription factor comprising three domains: an N-terminus dimerization domain, a highly conserved DNA-binding domain, and a C-terminus transactivation domain. Genetic changes comprise *HNF1B* intragenic mutations (50%) or a 1.4-Mb deletion at chromosome 17q12 including the entire *HNF1B* gene [9–11]. More than 200 *HNF1B* mutations have been reported including missense, nonsense, frameshift, splice-site mutations, and single exon deletion/duplication [12–17]. Mutations are scattered across the gene

containing nine exons, but they cluster predominantly in the first four exons, which encode the DNA-binding domain. Exons 2, 4, and the intron-2 splice site are hot-spot mutation sites [14]. Although characterized by an autosomal dominant inheritance, MODY5-related mutations often arise spontaneously [18]. No genotype/phenotype correlation exists, and there are differences in the clinical phenotypes caused by the same mutation [19].

Due to *HNF1B* expression in several tissues, the *HNF1B*-associated disease MODY5 is a multisystem disorder [14–16,20,21]. Renal cysts and diabetes are the most commonly observed features conferring the name of RCAD syndrome [14]. Kidney abnormalities consist of multicystic dysplastic kidneys, unilateral renal agenesis, renal interstitial fibrosis, collecting system malformations, and hypoplastic glomerulonephritic kidney disease [18,22–25]. Early-onset diabetes is the most common extra-renal manifestation [12,15,19,20]. The mean age of onset is ~24 years [14], but ranges from the neonatal period [26] to late middle age [19]. A recent multicenter retrospective cohort study showed that 79% of individuals with *HNF1B* mutations present with diabetes [16]. Patients display a fasting hyperglycemia and a reduced insulin response to glucose, and usually require insulin therapy in the first years following diagnosis [20,27–29]. Good diabetes control was achieved with insulin dosage, suggesting no overt insulin resistance. Anomalies of the exocrine pancreas constitute a common feature of *HNF1B* mutation carriers [14,20,30]. Pancreatic hypoplasia was often associated with ductal and acinar abnormalities [30,31]. Pancreas exocrine dysfunction, recently found in 76% of MODY5 patients [16], includes acute pancreatitis, calcifications characteristic of chronic pancreatitis or fecal elastase-1 deficiency [32]. Liver [20,24,33] and genital tract [20,29,34] abnormalities are additional MODY5 features. Two fetuses of ~7 months, with different mutations in exons 2 and 7, presented extremely severe and similar phenotypes [35]: bilateral enlarged polycystic kidneys, severe pancreas hypoplasia, and abnormal genital tract. Islets of Langerhans appeared slightly disorganized and the density of β-cells was moderately reduced, whereas acini were smaller and disorganized, with fibrosis. This provided evidence of differential gene-dosage requirements for *HNF1B* in human pancreas. Most MODY-causative genes encode transcription factors expressed in pancreatic β-cells, such as *HNF4A*, *HNF1A*, *PDX1*, and *PAX4*. By contrast, *HNF1B* is not expressed in mature β-cells [36–39]. It is expressed during development of the pancreas, kidney, liver, and genitourinary tract. *Hnf1b* is expressed in pancreatic multipotent progenitors by E9 in mice and lack of *Hnf1b* in the epiblast led to pancreas agenesis and lethality [36]. Around E12.5, *Hnf1b* becomes restricted to bipotent progenitors, giving rise to endocrine and ductal cells. Conditional inactivation of *Hnf1b* during embryogenesis led to pancreas hypoplasia associated with cystic ducts, loss of acinar cells, and lack of endocrine cells. Hnf1b is required for the expression of the pro-endocrine factor

Neurog3, a direct target of Hnf1b [40]. After birth, *Hnf1b* is expressed only in ductal cells [36–38] and post-natal *Hnf1b* inactivation in ductal cells led to chronic pancreatitis and neoplasia in adults [41]. Mutants showed dilatation of ducts, polarity defects, loss of acinar cells, acinar-to-ductal metaplasia (ADM), lipomatosis, macrophage infiltration, and fibrosis. This was associated with downregulation of cystic disease-associated genes, loss of primary cilia, and upregulation of signaling pathways [41].

Genetically heterozygous mutants of *Hnf1b* showed no reduction in native *Hnf1b* transcripts or proteins, and no phenotype [13,36,40,42]. There is therefore no truly heterozygous mouse mutant for *Hnf1b*, probably due to a compensatory phenomenon, which is not understood. A suitable mouse model is lacking to phenocopy the human HNF1B/MODY5 syndrome and dissect the molecular mechanisms. Here, we present a MODY5 mouse model generated through insertion of an *HNF1B* human splicing mutation identified in several patients at the intron-2 splice donor site (c.544±1G≥T; or ≤IVS2nt± 1G≥T) [20,43–45]. Importantly, this *Hnf1b*$^{sp2/+}$ mouse model recapitulates the pancreatic MODY5 clinical features, allowing exploration of MODY5 endocrine and exocrine defects.

Materials and methods

Mouse transgenic line

Hnf1b$^{sp2/+}$ mice were generated within the GIS Maladies Rares and Institut Clinique de la Souris (ICS). The *HNF1B* human mutation located in the splice donor site of intron-2 c.544+1G>T (IVS2nt+1G>T) was introduced by targeted homologous recombination. *Hnf1b*$^{sp2/+}$ mice were maintained in a mixed background: 129/Sv:C57BL/6N. Wild-type (WT) mice used as controls were littermates of *Hnf1b*$^{sp2/+}$ mice generated from crosses between *Hnf1b*$^{+/+}$ and *Hnf1b*$^{sp2/+}$ mice. Animal experiments were conducted in accordance with European and French ethical legal guidelines and the local ethical committee (Charles Darwin n°5, approval number: 01508).

Histology, immunohistochemistry, and immunofluorescence

Pancreases were fixed in 4% formaldehyde overnight and embedded in paraffin. Sections cut at 7 μm were processed for histological staining, immunofluorescence or immunohistochemistry as described previously [41]. The primary antibodies used are listed in supplementary material, Table S1. Fibrosis was assessed using Masson's trichrome staining and quantified with ImageJ ($n = 3$, at least six sections per n). The length of cilia was measured following dual Sox9/acetylated α-tubulin immunofluorescence and quantified using ImageJ ($n = 3$, ~50 cilia per n). Acinar cell proliferation was quantified from amylase/phospho-histone H3 (PHH3)

immunofluorescence, with the number of mitotic acinar cells being divided by the surface area of amylase staining ($n = 3$, at least two sections per n).

RNA extraction, reverse transcription, and quantitative PCR (RT-qPCR)

Total RNA from pancreas was isolated using an RNeasy Mini Kit (Qiagen, Düsseldorf, Germany) and reverse-transcribed using a SuperScript RT II Kit (Invitrogen, Thermo Fisher Scientific, Waltham, MA, USA). The qPCR reactions were performed using SYBR Green Master Mix (EurobioGreen qPCR Mix, Hi-ROX; Eurobio Ingen, Les Ulis, France). Expression levels were calculated using the method of relative quantification, normalized to *Ppia* and relative to WT cDNA from E15.5 pancreases. Values are shown as mean ± SEM. Primer sequences are provided in supplementary material, Table S2.

Western immunoblotting

Pancreatic extracts were prepared from $Hnf1b^{sp2/+}$ mice at postnatal day 8 (P8) using Tissue Extraction Reagent (Invitrogen Thermo Fisher Scientific) and Protease Inhibitor Cocktail (Thermo Fisher Scientific) in a Qiagen Tissuelyser followed by sonication (Bioruptor®; Diagenode, Liège, Belgium). Extracts were resolved on 4–12% precast sodium dodecyl sulfate-polyacrylamide electrophoresis gels (Invitrogen Thermo Fisher Scientific) and transferred onto nitrocellulose membranes (BioTrace™ NT; Pall Corporation, Port Washington, NY, USA). Hnf1b was detected with our previously validated homemade rabbit polyclonal antibody, against residues 39–89 of the mouse Hnf1b protein (1:2000 [35]), and β-actin with rabbit polyclonal antibody (A2066; Sigma-Aldrich, St Louis, MO, USA; 1:2000). Detection was performed with SuperSignal™ West Femto (Thermo Fisher Scientific).

Glucose and insulin tolerance tests

For intraperitoneal glucose tolerance tests (IPGTTs), glucose was injected intraperitoneally (2 g/kg body weight) to overnight-fasted mice. For insulin tolerance tests (ITTs), insulin (Novo Nordisk, Gladsaxe, Denmark; 100 UI/ml) was injected intraperitoneally (1 unit/kg body weight) after a 6-h fast. Plasma insulin levels during IPGTTs were assessed with mouse insulin ELISA (Eurobio Ingen).

Pancreatic insulin content

The entire pancreas was homogenized in acid–ethanol solution (2% HCl, 80% ethanol), incubated overnight at $-20\,°C$, and then centrifuged at $4\,°C$ for 10 min [46]. The supernatant was diluted and neutralized in PBS and subjected to ELISA for mouse insulin (Eurobio Ingen). Insulin content was normalized to the protein concentration of pancreatic lysate, to pancreatic weight or to mouse weight.

Mouse islet isolation and cell culture

Islets of adult mice were isolated with collagenase XI (1 mg/ml; Sigma-Aldrich C7657) [47], separated on Histopaque gradient (Sigma-Aldrich), and hand-picked under a binocular microscope. Islets were cultured in RPMI supplemented with Glutamax, 10% fetal calf serum, and 1% penicillin/streptomycin stock solution. Islets were placed in a 24-well plate insert (30 islets per insert), incubated for 1 h under basal conditions in Krebs-Ringer bicarbonate HEPES (KRBH) buffer at 2.8 mm glucose concentration (low), and insulin secretion was induced by incubation for 1 h at 16.7 mm glucose (high). Insulin secretion was analyzed using an ELISA kit (Eurobio Ingen) ($n \geq 7$, in triplicates).

Optical projection tomography (OPT)

Pancreases from adult mice (4 months old) were fixed in 4% paraformaldehyde for 2.5 h and dehydrated in methanol. The OPT imaging protocol was as described previously [48,49] for the pancreatic dorsal, splenic, and gastric lobes [50]. Samples were freeze-thawed to increase permeability, bleached (in DMSO, methanol, and hydrogen peroxide; 1:2:3, respectively; Thermo Fisher Scientific) to reduce endogenous fluorescence, and then stained with primary guinea pig anti-insulin (DAKO, Glostrup, Denmark; A0564, 1:500) and secondary goat Alexa594 anti-guinea pig (Molecular Probes, Thermo Fisher Scientific A11076) antibodies. Samples were mounted in 1.5% Low-melting SeaPlaque™ Agarose (Lonza, Walkersville, MD, USA) and optically cleared using a 1:2 dilution of benzyl alcohol and benzyl benzoate, respectively (Acros Organics, ThermoFisher Scientific). OPT imaging was performed using a BiOPTonics SkyScanner 3001. Image data sets were processed using a contrast limited adaptive histogram equalization (CLAHE [51]), and a post-acquisition misalignment correction was implemented using discrete Fourier transform alignment (DFTA [52]). The processed and aligned frontal projection images were reconstructed to tomographic sections (SkyScan NRecon; Bruker, Billerica, MA, USA) and uploaded to Imaris (Bitplane, Belfast, UK).

Caerulein treatment

Three-month-old mice were injected with caerulein (C9026; Sigma-Aldrich), a decapeptide analogue of the pancreatic secretagogue cholecystokinin, at a dose of 75 µg/kg. Caerulein was administered by intraperitoneal injections hourly, 7 times a day, for two consecutive days. Pancreases were harvested before caerulein injection at day 0 (D0), when acute pancreatitis was induced 3 days after the first injection (D3), and when the pancreas was almost fully regenerated at D7.

Statistical analysis

Statistical analyses were carried out using GraphPad Prism 6.0 (GraphPad Software, San Diego, CA, USA). Statistical significance ($p < 0.05$) was determined using

Student's *t*-test or the non-parametric Mann–Whitney U-test when appropriate.

Results

Generation of *Hnf1b*$^{sp2/+}$ mice, a mouse model reproducing human pathogenic *HNF1B* splicing mutation

A G-to-T point mutation was introduced by homologous recombination at the intron-2 splice donor site, mimicking the human c.544+1G>T (<IVS2nt+1G>T) mutation (Figure 1A). This mutation resulted in a deletion of the splice donor site of intron 2, and skipping of exon 2 would produce an out-of-frame splice product from exon 1 to exon 3. This mutated allele was defined as *Hnf1b*^{sp2}. Heterozygous *Hnf1b*$^{sp2/+}$ mice were born with the expected Mendelian ratio and grew normally (supplementary material, Figure S1). mRNA transcripts were analyzed using RT-PCR in the region encompassing exons 1–3. The expected PCR products corresponding to *Hnf1b* isoforms A and B were obtained in both WT and *Hnf1b*$^{sp2/+}$ pancreases. Novel transcripts, corresponding to isoforms A and B in which exon 2 was deleted, were identified in *Hnf1b*$^{sp2/+}$ (Figure 1B). These *Hnf1b* variants lacking exon 2 are consistent with analysis in human patients [44]. After sequencing, other variants lacking the last 32 bp of exon 2 resulting from the use of another cryptic splicing site within exon 2 were also identified (supplementary material, Figure S2). All the *Hnf1b* variants were predicted to result in premature termination of the Hnf1b protein, with lack of the DNA-binding domain and the transactivation domain. Using RT-qPCR, analysis of the native *Hnf1b* transcripts showed a 39% and 38% decrease in *Hnf1b*$^{sp2/+}$ pancreases compared with WT at E15.5 and E17.5, respectively (Figure 1C). In correlation, WB analysis showed a 30% decrease in the amount of native Hnf1b proteins in *Hnf1b*$^{sp2/+}$ pancreases (Figure 1D,E). The predicted truncated Hnf1b proteins in *Hnf1b*$^{sp2/+}$ pancreases were undetectable (Figure 1D). Thus, the G>T *HNF1b* point mutation introduced into these mice results in a significant decrease in *Hnf1b* expression, mimicking the impact of the IVSnt+G>T mutation in humans, and suggesting that this might be a promising model for exploring the pathophysiology of MODY5.

Impaired glucose tolerance in *Hnf1b*$^{sp2/+}$ mice

IPGTT was performed to assess glucose homeostasis. The blood glucose level of 6-week-old *Hnf1b*$^{sp2/+}$ mice was significantly increased at 60 min in comparison to WT (Figure 2A). In 12- and 24-week-old *Hnf1b*$^{sp2/+}$ mice, the blood glucose level was significantly higher than that of WT at all time points, as well as the corresponding AUC (area under the curve) (Figure 2B,C). Plasma insulin levels were measured at 12 weeks and showed that less insulin was secreted in *Hnf1b*$^{sp2/+}$ mice compared with WT during IPGTT (Figure 2D).

Hnf1b$^{sp2/+}$ mice also displayed a higher glucose level compared with WT in both fed and fasted states (Figure 2E,F). ITT performed on 24-week-old animals revealed no difference in peripheral insulin sensitivity between *Hnf1b*$^{sp2/+}$ and WT (Figure 2G), suggesting that the increased blood glucose level in *Hnf1b*$^{sp2/+}$ mice was not associated with insulin resistance of peripheral organs. Thus, *Hnf1b*$^{sp2/+}$ mice were glucose-intolerant, with hyperglycemia that progressed with age.

Reduced pancreatic insulin content is associated with a reduced volume and number of large islets in *Hnf1b*$^{sp2/+}$ mice

We investigated the cause of glucose intolerance and found a 65% decrease in pancreatic insulin content in *Hnf1b*$^{sp2/+}$ mice compared with WT (Figure 3A). We examined glucose-stimulated insulin secretion (GSIS) as a measure of β-cell function. Isolated islets were incubated with a basal (2.8 mM) or a high (16.7 mM) concentration of glucose. In both conditions, islets isolated from *Hnf1b*$^{sp2/+}$ pancreases secreted levels of insulin similar to those of WT (Figure 3B). Moreover, no difference in the expression of β-cell markers was observed in *Hnf1b*$^{sp2/+}$ and WT isolated islets (Figure 3C). This suggested that the decrease of pancreatic insulin content of *Hnf1b*$^{sp2/+}$ mice was not due to β-cell dysfunction. We then assessed the volume and number of islets by 3D imaging optical projection tomography (OPT) [53], a method for direct quantification and 3D spatial assessment of β-cell mass. Small ($<1 \times 10^6$ μm^3), medium (1×10^6–5×10^6 μm^3), and large ($>5 \times 10^6$ μm^3) islets were reconstructed (supplementary material, Movies S1-S6) and quantified based on the signal from insulin-specific antibody (Figure 3D). A 20% decrease of the total islet volume was observed in *Hnf1b*$^{sp2/+}$ pancreases compared with WT (Figure 3E). Moreover, we found a 28% decrease in the volume of large islets (Figure 3F). This specific decrease in the volume of large islets was observed in duodenal (38%) and splenic (26%) lobes of *Hnf1b*$^{sp2/+}$ pancreases (Figure 3G). The volume per large islet was also significantly decreased (Figure 3H). This was correlated with a 22% decrease in the number of large islets in *Hnf1b*$^{sp2/+}$ pancreases (Figure 3I). Taken together, these data show that *Hnf1b*$^{sp2/+}$ pancreases have a decreased number and volume of large islets leading to reduced pancreatic insulin content.

Downregulation of endocrine markers during *Hnf1b*$^{sp2/+}$ pancreas development

Since postnatal islets do not express *Hnf1b*, which is restricted to ductal cells from ~E14.5 [36–38], and based on the essential role of *Hnf1b* in endocrine commitment [40], we hypothesized that the endocrine defects observed could be due to impaired islet development. We found a 32% and a 27% decrease in *Neurog3* expression at E15.5 and E17.5, respectively, in *Hnf1b*$^{sp2/+}$ pancreases compared with WT (Figure 4A). This result was consistent with our finding that Hnf1b is a direct activator of *Neurog3* [40]. In correlation, we found an approximately 35%
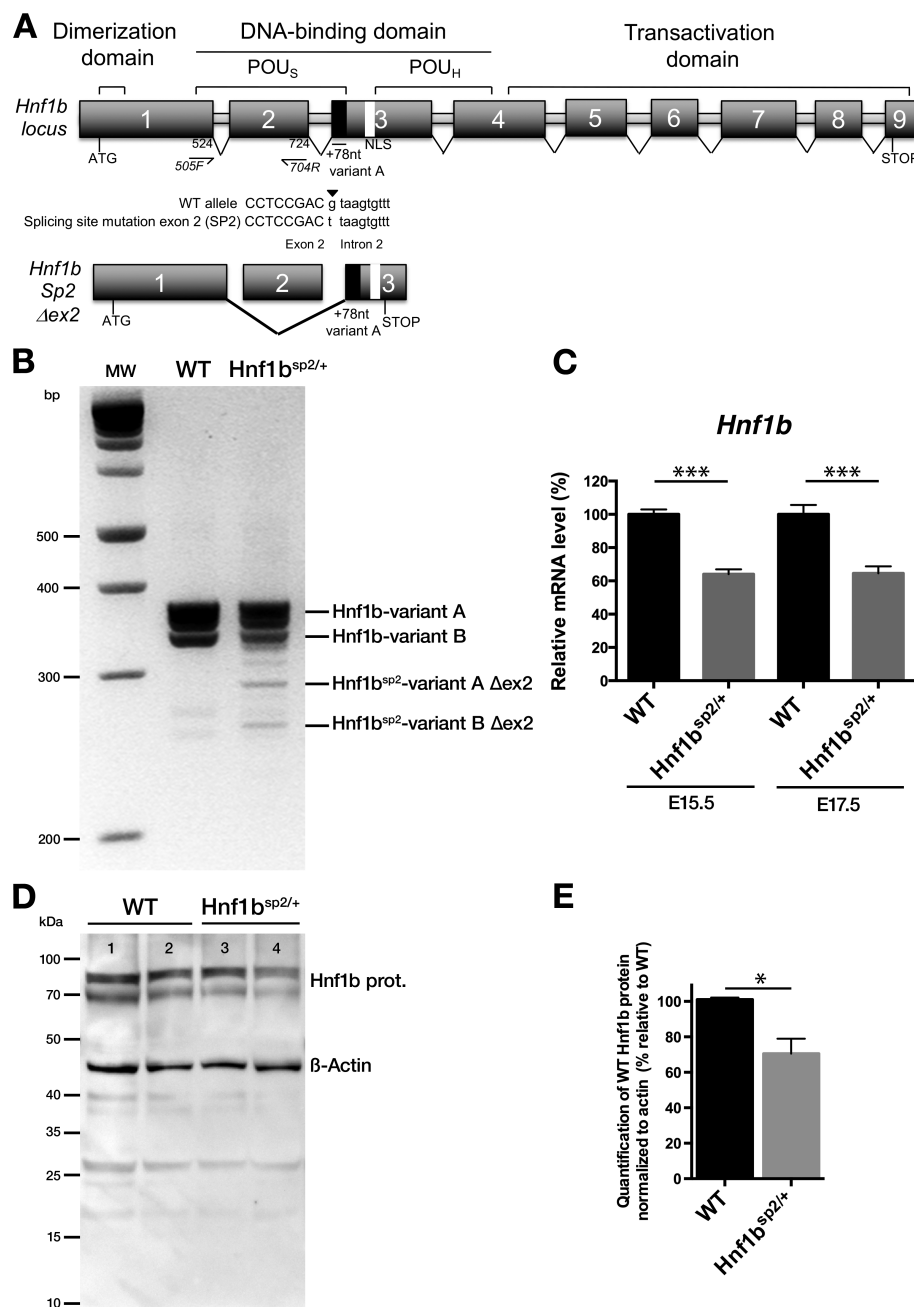
Figure 1. Generation of the *Hnf1b* intron-2 splice-mutant mice. (A) Genomic organization of the *Hnf1b* locus showing the nine coding exons and the corresponding functional domains of Hnf1b protein. The DNA-binding domain is divided into a POU-specific domain (POU_S) and a POU-homeodomain (POU_H). The 78 nt specifically present in variant A and the nuclear localization signal (NLS) are indicated. The locations of the primers used for measurement of full-length *Hnf1b* transcripts by RT-qPCR in C are indicated (forward primer 505F in exon 1 and reverse primer 704R in exon 2). The G-to-T mutation introduced in intron 2 is shown, as well as the *Hnf1b* variant A and variant B transcripts lacking exon 2 corresponding to truncated proteins in *Hnf1b*[sp2/+] mice. (B) RT-PCR analysis of *Hnf1b* transcripts in WT and *Hnf1b*[sp2/+] pancreases. Representative RT-PCR from E15.5 pancreases of WT and *Hnf1b*[sp2/+], using primers located in exon 1 and exon 3 with 37 cycles of amplification. WT pancreases express *Hnf1b* variants A and B, while *Hnf1b*[sp2/+] pancreases express additional abnormal spliced transcripts notably corresponding to variants A and B lacking exon 2. (C) RT-qPCR analysis showing a 38% decrease in the expression of normal *Hnf1b* transcripts in *Hnf1b*[sp2/+] pancreases, compared with WT, at E15.5 (WT, $n = 8$; *Hnf1b*[sp2/+], $n = 16$) and E17.5 (WT, $n = 9$; *Hnf1b*[sp2/+], $n = 13$). (D) Western blotting analysis of Hnf1b proteins in WT (lanes 1 and 2) and *Hnf1b*[sp2/+] pancreases (lanes 3 and 4) at P8. No truncated Hnf1b proteins were detectable in *Hnf1b*[sp2/+] pancreases. (E) Quantification showed a 30% decrease in the amount of native Hnf1b proteins with β-actin normalization (WT, $n = 4$; *Hnf1b*[sp2/+], $n = 4$). *$p < 0.05$; ***$p < 0.001$.

decrease in the expression of endocrine markers at E17.5, whereas the expression of acinar and ductal markers was unchanged (Figure 4B). Thus, *Hnf1b*[sp2/+] mice displayed an altered development of endocrine cells.

Hnf1b[sp2/+] mice develop chronic pancreatitis

We next investigated the exocrine phenotype of *Hnf1b*[sp2/+] mice. Histological analysis revealed altered exocrine tissue with few acinar lobules (Figure 5A,B). In correlation,
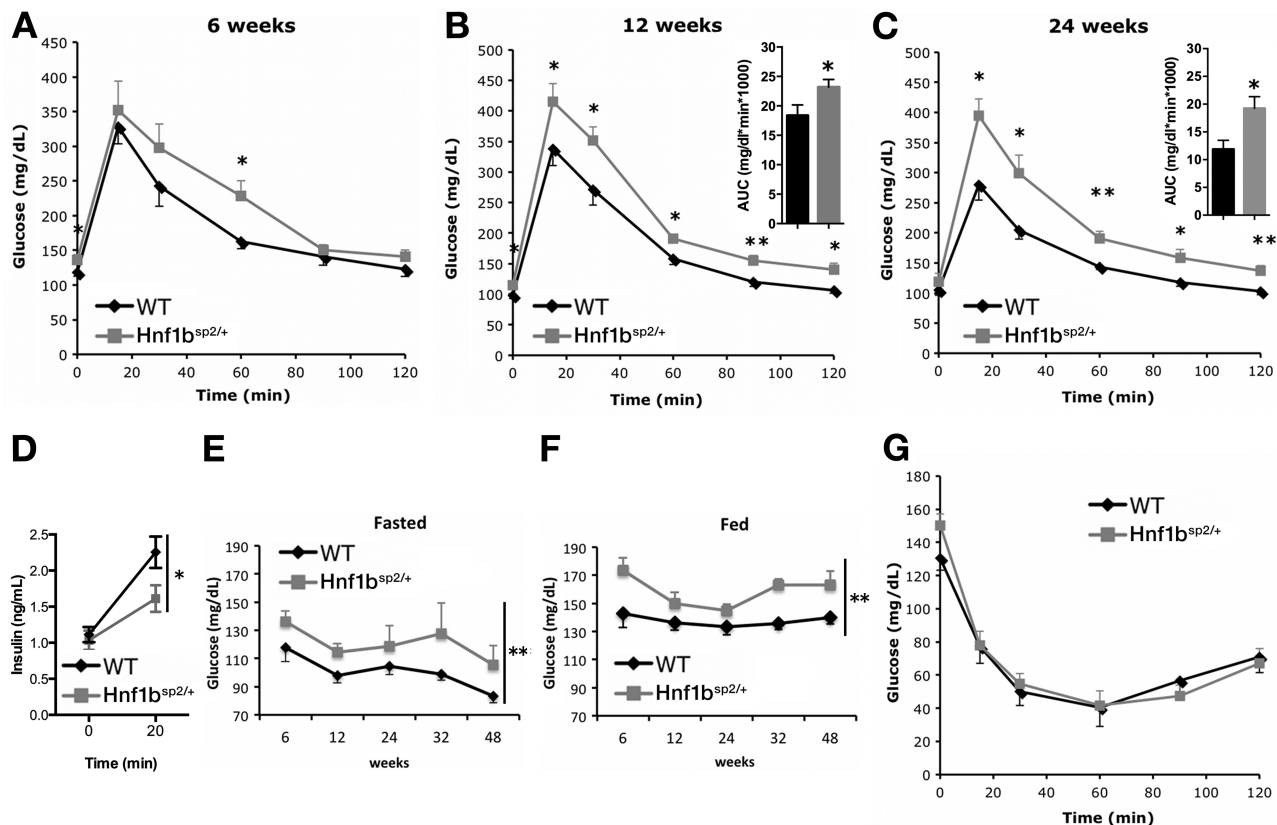
Figure 2. *Hnf1b$^{sp2/+}$* mice are glucose-intolerant but not insulin-resistant. (A–C) Intraperitoneal glucose tolerance test (IPGTT) in 6-, 12-, and 24-week-old *Hnf1b$^{sp2/+}$* (grey line) and WT (black line) mice. The corresponding area under the curve (AUC) is shown for 12- and 24-week-old animals. (D) Plasma insulin levels measured at 12 weeks of age at the beginning of the IPGTT (T0) and at 20 min (T20). (E) Overnight-fasted blood glucose levels of WT (black line) and *Hnf1b$^{sp2/+}$* (grey line) mice between 6 and 48 weeks. (F) Morning-fed blood glucose values of WT (black line) and *Hnf1b$^{sp2/+}$* (grey line) mice between 6 and 48 weeks. (G) Insulin tolerance test (ITT) in 24-week-old *Hnf1b$^{sp2/+}$* (grey line) and WT (black line) mice. WT, $n = 8$; *Hnf1b$^{sp2/+}$*, $n = 6$. *$p < 0.05$; **$p < 0.01$.

expression of acinar markers was reduced by ~80% at 12 months (Figure 5C). Hematoxylin and eosin (H&E) staining showed many duct-like structures within the *Hnf1b$^{sp2/+}$* acinar tissue (Figure 5D,E). Following dual Sox9/amylase immunofluorescence, we observed nuclear localization of the ductal marker Sox9 in many amylase$^+$ acinar cells in *Hnf1b$^{sp2/+}$* pancreases, demonstrating ADM (Figure 5F,G). *Hnf1b$^{sp2/+}$* pancreases were also filled with adipocytes, as shown by immunostaining for Fabp4 (Figure 5H,I). This correlates with the high upregulation (25.7-fold) of *Pparg*, a key player in adipocyte differentiation (Figure 5J). F4/80 immunostaining revealed immune infiltrates consisting of macrophages (Figure 5K, L) and correlated with a 7.4-fold increase in the expression of *Adgre1*, the gene encoding F4/80 expression (Figure 5M). Expression of *Cd2* and *Cd19*, markers of T and B cells, respectively, as well as expression of cytokines and chemokines, was also increased (Figure 5M), showing the high level of inflammation of *Hnf1b$^{sp2/+}$* pancreases. Moreover, extensive fibrosis was observed, as shown using Masson's trichrome, staining collagenous fibers in green (Figure 5N,O), and quantification of fibrotic areas (Figure 5P). The mesenchymal marker vimentin was localized ectopically in *Hnf1b$^{sp2/+}$* pancreases (Figure 5Q,R), associated with increased mRNA expression (11.8-fold) (Figure 5S). *Tgfb1*, a master regulator of fibrogenesis,

was strongly upregulated (7.4-fold). Fibrotic and desmoplasia-associated markers were also overexpressed, such as *Cdh2* (encoding N-cadherin) (3.9-fold), *Col1a1* (10.4-fold), and *Acta2*, encoding α-SMA (15.1-fold) (Figure 5S). Strong and ectopic staining for Ccn2 (also known as Ctgf) was observed in *Hnf1b$^{sp2/+}$* acinar cells (Figure 5T,U); CCN2 is known to cooperate with TGFβ to promote fibrosis and inflammation [54]. We found an elevated level of expression of both *Ccn2* (8.1-fold) and *Ccn1*, known also as *Cyr61* (12.1-fold) (Figure 5V); *CCN* genes are known to stimulate fibrogenic pathways in pancreatic stellate cells during pancreatitis [54]. Thus, *Hnf1b$^{sp2/+}$* pancreases exhibit acinar cell loss, ADM, lipomatosis, immune infiltration, and fibrosis, showing that *Hnf1b$^{sp2/+}$* mice develop chronic pancreatitis.

Defective cilia in *Hnf1b$^{sp2/+}$* ductal cells

Neonatal inactivation of *Hnf1b* led to the loss of ductal cells primary cilia, resulting in a non-cell autonomous loss of acinar cells [41]. We therefore tested whether the chronic pancreatitis observed in *Hnf1b$^{sp2/+}$* mice could be initiated by a defect in the cilia of ductal cells. Chronic pancreatitis develops progressively, as shown by the decrease in pancreas weight/body weight ratio,

ranging from −19% at 5 months to −38% at 12 months (Figure 6A). We performed an analysis at 3 months, a stage at which the overall morphology of the pancreas was not altered (Figure 6B,C). The primary cilia of ductal cells were visualized using dual immunofluorescence for Sox9 and acetylated α-tubulin (a modification of the
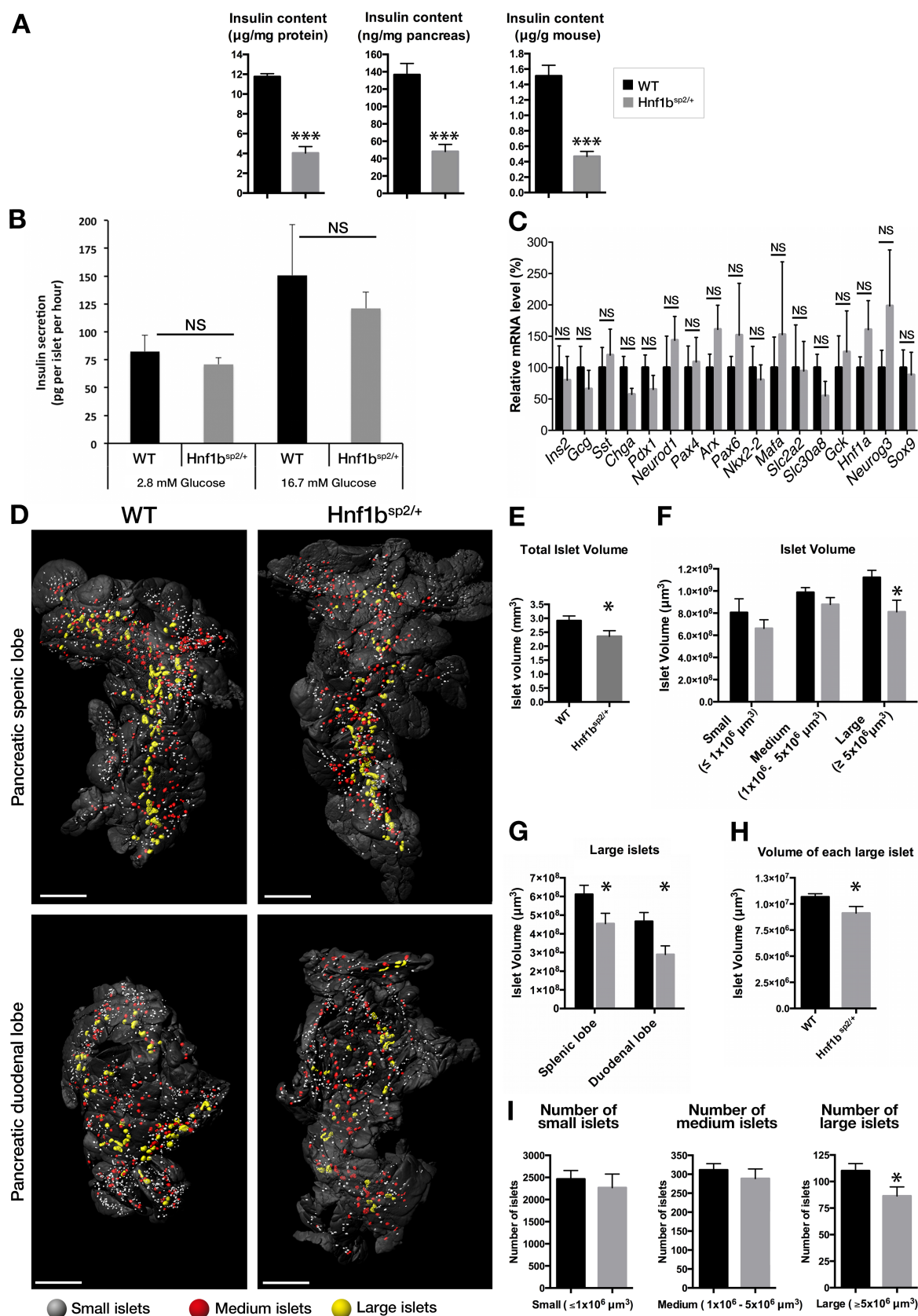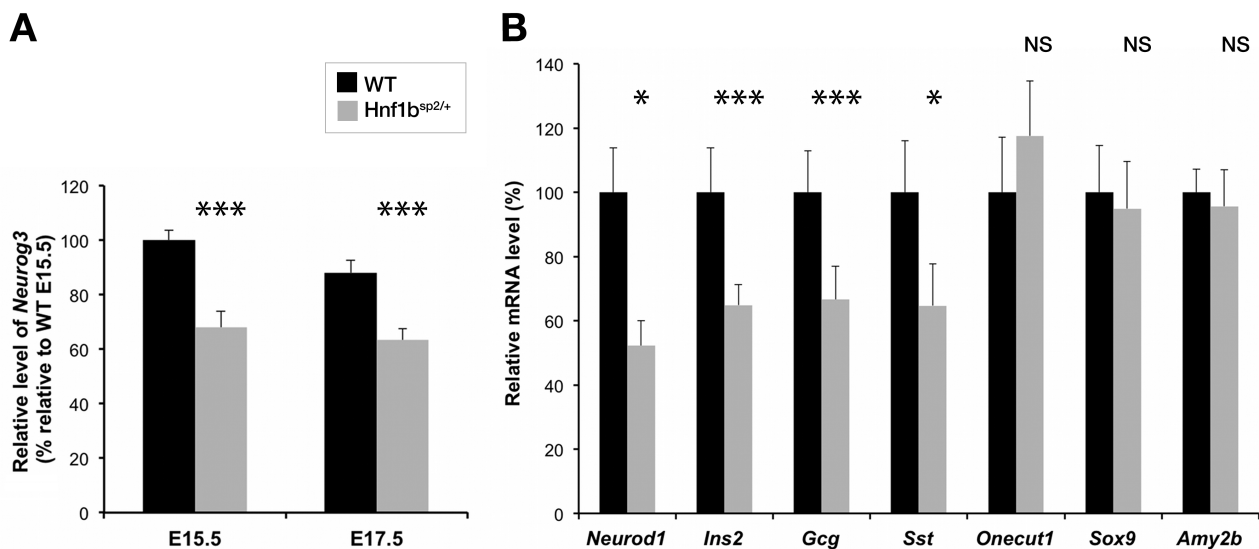

Figure 3 Legend on next page.

Figure 4. Decreased *Ngn3* and endocrine marker expressions in *Hnf1b*$^{sp2/+}$ embryonic pancreas. (A) RT-qPCR analysis of the pro-endocrine gene *Neurog3* in *Hnf1b*$^{sp2/+}$ (grey) and WT (black) pancreases at E15.5 (WT, $n = 8$; *Hnf1b*$^{sp2/+}$, $n = 16$) and E17.5 (WT, $n = 8$; *Hnf1b*$^{sp2/+}$, $n = 12$). (B) RT-qPCR analysis of markers of endocrine (*Neurod1, Ins2, Gcg/Glucagon, Sst/Somatostatin*), ductal (*Onecut1/Hnf6, Sox9*), and acinar (*Amy2b/ Amylase*) gene expression in WT (black, $n = 17$) and *Hnf1b*$^{sp2/+}$ (grey, $n = 17$) mice at E17.5. *$p < 0.05$; **$p < 0.01$; ***$p < 0.001$.

tubulin present on primary cilium axoneme). Primary cilia appeared shorter (Figure 6D,E) and quantification showed a dramatic decrease (-71%) in the cilia length of *Hnf1b*$^{sp2/+}$ ductal cells compared with WT (Figure 6F). At this stage, defective cilia of ductal cells were associated with a decreased proliferation rate (-47%) of acinar cells, as shown by quantification from dual PHH3/amylase immunofluorescence (Figure 6G– I), contributing to the loss of acinar cells. We previously observed that *Hnf1b* conditional inactivation in adult pancreatic ductal cells impaired acinar cell regeneration following caerulein-induced pancreatitis [41]. There- fore, we wondered if acinar cell regeneration would be impaired after induction of acute pancreatitis in 3-month-old *Hnf1b*$^{sp2/+}$ mice by two consecutive days of treatment with the secretagogue caerulein (Figure 6J). We followed acinar regeneration by dual immunofluorescence for Sox9/amylase (Figure 6K–P). Before caerulein treatment (D0), we found no difference between WT and *Hnf1b*$^{sp2/+}$ pancreases (Figure 6K,L). Three days after the first injection (D3), both WT and *Hnf1b*$^{sp2/+}$ pancreases exhibited widespread ADM revealed by ectopic localization of Sox9 in the nuclei

of many amylase-positive acinar cells (Figure 6M,N). WT mice were mostly recovered at D7, whereas large ADM areas were still observed in *Hnf1b*$^{sp2/+}$ pancreases (Figure 6F,G), showing impaired acinar cell regenera- tion in young *Hnf1b*$^{sp2/+}$ mice.

Discussion

Investigating MODY5 pathology is complex due to the scarcity of patients, the phenotypic heterogeneity, and the lack of a suitable mouse model. Here, we show that *Hnf1b*$^{sp2/+}$ mice, a unique murine model of MODY5 established by insertion of a human *HNF1B* splicing point mutation, reproduce the pancreatic defects of MODY5 patients. The mouse phenotype appears more homogeneous than that in humans, probably due to less variability in modifier genes and environmental factors. Unlike *Hnf1b*$^{+/-}$ mice that did not show a decrease in *Hnf1b* mRNA expression because of a compensatory mechanism, which might be due to locus conformation, especially with LacZ insertion [13,36,40,42], *Hnf1b*$^{sp2/+}$ heterozygous mice constitute an appropriate model for

Figure 3. Decreased pancreatic insulin content and islet volume in *Hnf1b*$^{sp2/+}$ mice. (A) Pancreatic insulin content in 8-month-old *Hnf1b*$^{sp2/+}$ (grey, $n = 7$) and WT (black, $n = 3$) mice, reported either to the protein amount, to the pancreas weight or to the mouse weight. (B) Insulin secretion from *Hnf1b*$^{sp2/+}$ isolated islets (grey, $n = 7$) and WT (black, $n = 8$) cultured in basal (2.8 mM glucose) or glucose-stimulated (16.7 mM glucose) conditions. (C) RT-qPCR analysis for β-cell markers in *Hnf1b*$^{sp2/+}$ (grey, $n = 6$) and WT (black, $n = 7$) isolated islets. (D) Isosurface rendered optical projection tomography (OPT) images of representative duodenal and splenic lobes of *Hnf1b*$^{sp2/+}$ and WT pancreases of 4– month-old mice. Individual islet volumes were reconstructed based on the signal from insulin-specific antibody and were pseudo-colored to highlight the distribution of small [$<1 \times 10^6$ μm^3 (white)], medium [1×10^6–5×10^6 μm^3 (red)], and large [$>5 \times 10^6$ μm^3 (yellow)] islets. (E) Quantification of total islet volume in *Hnf1b*$^{sp2/+}$ (grey) and WT (black) pancreases. (F) Quantification of small, medium, and large islet total volumes in *Hnf1b*$^{sp2/+}$ (grey) and WT (black) pancreases. (G) Quantification of large islets in splenic and duodenal lobes in *Hnf1b*$^{sp2/+}$ (grey) and WT (black) pancreases. (H) Mean volume of each large islet determined by the ratio of large islet volume to large islet number in *Hnf1b*$^{sp2/+}$ (grey) and WT (black) pancreases. (I) Quantification of small, medium, and large islet numbers in *Hnf1b*$^{sp2/+}$ (grey) and WT (black) pancreases. WT, $n = 7$; *Hnf1b*$^{sp2/+}$, $n = 7$. *$p < 0.05$; ***$p < 0.001$; NS, not significant. Scale bar: 1 mm.

the disease. The renal disorders of *Hnf1b^sp2/+* mice will be described in a separate report (Niborsky *et al*, personal communication, 2021).

Hnf1b^sp2/+ mice mimicking the human c.544+1G>T (<IVS2nt+1G>T) mutation displayed mutant transcripts harboring a premature termination codon. This theoretically

Figure 5 Legend on next page.

leads to inactive truncated proteins, without DNA-binding and transactivation domains. Mutated splice variants were less abundant than the native transcripts. The nonsense-mediated mRNA decay (NMD) surveillance pathway can degrade such transcripts. However, because cycloheximide (an NMD inhibitor) failed to alter the frequencies of the corresponding human *HNF1B* transcripts [44], the lower relative level of mutant splice variants is unlikely to be due to NMD. It is more likely that their stability is compromised by other mechanisms, such as conformational changes in their tertiary structure [55]. We failed to detect the truncated proteins produced by these alternative transcripts probably because they are unstable, as previously shown for truncated proteins generated from transcripts that escaped NMD [56]. *Hnf1b*^{sp2/+} mice showed a significant decrease in *Hnf1b* mRNA expression (~40%), *Hnf1b* haploinsufficiency thus constituting the disease mechanism.

Hnf1b^{sp2/+} mice develop diabetes associated with reduced β-cell mass caused by embryonic endocrine defect

The glucose intolerance observed in *Hnf1b*^{sp2/+} mice arose from 6 weeks of age and progressed with age. This correlates with glucose tolerance tests in MODY5 patients showing a reduced insulin response to glucose [20,27–29], and a progression towards a diabetic profile [12]. Insulin resistance is an additional feature of some MODY5 patients, with decreased insulin sensitivity [57,58]. Overexpression of miR-802 in the liver impaired glucose metabolism through silencing of *Hnf1b*, revealing a role for Hnf1b in hepatic insulin sensitivity [42]. ITT analysis of *Hnf1b*^{sp2/+} mice showed no insulin resistance. However, the liver phenotype of *Hnf1b*^{sp2/+} mice and how Hnf1b could control hepatic glucose metabolism will be analyzed in a further study.

Unlike *Hnf1a* and *Hnf4a*, *Hnf1b* is not expressed in pancreatic β-cells [36–39]. Therefore, MODY5 cannot be due to intrinsic β-cell dysfunction caused by altered regulation of the HNF1B target genes in β-cells. Even though a mouse study has reported that conditional inactivation of *Hnf1b* in β-cells led to glucose intolerance [59], it is now known that the RIP-Cre reporter line used alone caused glucose intolerance [60]. *Hnf1b*^{sp2/+} mice showed a 65% decrease in insulin content and morphometric analyses an approximately 20% decrease in total

islet volume. Large islets of *Hnf1b*^{sp2/+} mice were fewer and smaller than in WT, with an approximately 30% decrease in volume, leading to the significant decrease in pancreatic insulin content. This is in accordance with the observation that large and medium islets contribute to the majority of total β-cell mass [50]. The decrease in the size of large islets may also reflect an overall decrease in the size of all islets, with large islets becoming medium, and medium ones becoming small. This may be due to a defect in islet morphogenesis, suggesting a developmental role of *Hnf1b* in islet formation. This possibility is supported by our observation that *Hnf1b* conditional inactivation in pancreatic progenitors and embryonic ducts resulted in decreased expression of *Neurog3* [40]. Endocrine cells derived from progenitors that transiently express high levels of *Neurog3* [61,62] and loss of Neurog3 activity disrupts endocrine islet cell differentiation in mice [63,64] and pigs [65]. *Hnf1b*^{sp2/+} mice exhibited an approximately 30% decrease in *Neurog3* expression during embryonic development, associated with decreased expression of endocrine markers. Therefore, even if the manifestation of the disease is after birth, the endocrine defects in MODY5 arise from defects in embryogenesis. The phenotype of *Hnf1b*^{sp2/+} mice is reminiscent of the one of mouse models harboring a reduced *Neurog3* dosage that led to glucose intolerance, unaltered insulin sensitivity and insulin secretion capability of isolated islets, but decreased islet mass, with reduced abundance and size of islets [66]. This showed that islet mass was predominantly determined by the controlled allocation of pancreatic progenitors to the endocrine lineage during embryogenesis [67]. In humans, *NEUROG3* mutations are associated with permanent neonatal diabetes mellitus (PNDM) or delayed onset of insulin-dependent diabetes mellitus (IDDM) [68,69]. The variability in the onset of MODY5 among patients might be correlated with their level of *NEUROG3* expression during fetal development.

It has recently been appreciated that even a moderate decrease in β-cell mass such as in *Hnf1b*^{sp2/+} mice can cause diabetes, and that a deficit in the β-cell volume is an early occurrence in T2D [70]. Most studies agree that a reduction in β-cell mass associated with T2D ranges from ~20% to ~60% [71,72]. Older-onset T1D subjects also showed a more preserved β-cell mass than expected, with up to 40% insulin-containing islets [73,74]. In T2D, the insulin content of human pancreas was reduced by ~30% [75,76] and islet number and volume by ~22–

Figure 5. *Hnf1b*^{sp2/+} mice develop chronic pancreatitis. (A, B) Global histology of WT and *Hnf1b*^{sp2/+} pancreases at 12 months. (C) RT-qPCR analysis of acinar marker genes in WT (black, *n* = 4) and *Hnf1b*^{sp2/+} (grey, *n* = 6) at 12 months. (D, E) Hematoxylin and eosin staining of WT and *Hnf1b*^{sp2/+} pancreases at 12 months. Scale bars: 100 μm. (F, G) Amylase (green) and Sox9 (red) immunofluorescence. (H, I) Adipocyte marker Fabp4 (green) immunofluorescence. Scale bars: 50 μm. (J) RT-qPCR for *Pparg*, a marker of adipogenesis. (K, L) Immunohistochemistry of immune infiltrates with the macrophage marker F4/80 (brown). Scale bars: 50 μm. (M) RT-qPCR for inflammatory markers. (N, O) Masson's trichrome staining. Collagen fibers are stained in green. Scale bars: 100 μm. (P) Quantification of fibrotic areas. (Q, R) Vimentin (brown) immunohistochemistry. Scale bars: 50 μm. (S) RT-qPCR for *Tgfb1*, *Cdh2* (encoding N-cadherin), *Vim*, *Col1a1*, and *Acta2*. (T, U) CTGF (brown) immunohistochemistry. Scale bars: 50 μm. (V) RT-qPCR for *Ctgf/Ccn2* and *Cyr61/Ccn1*. WT, *n* ≥ 3; *Hnf1b*^{sp2/+}, *n* ≥ 3 for histology, immunofluorescence, and immunohistochemistry; WT, *n* = 4; *Hnf1b*^{sp2/+}, *n* = 6 for RT-qPCR. *$p < 0.05$ **$p < 0.01$; ***$p < 0.001$.

30% [76–79]. T2D subjects displayed smaller islets [76,79,80], with a preferential loss of large islets suggesting that they ensure critical roles in glucose level regulation [81,82].

Results from our *Hnf1b*^{sp2/+} mice suggest that MODY5 diabetes may be due to a decrease in β-cells available at birth leading to a reduced β-cell mass with fewer large islets.
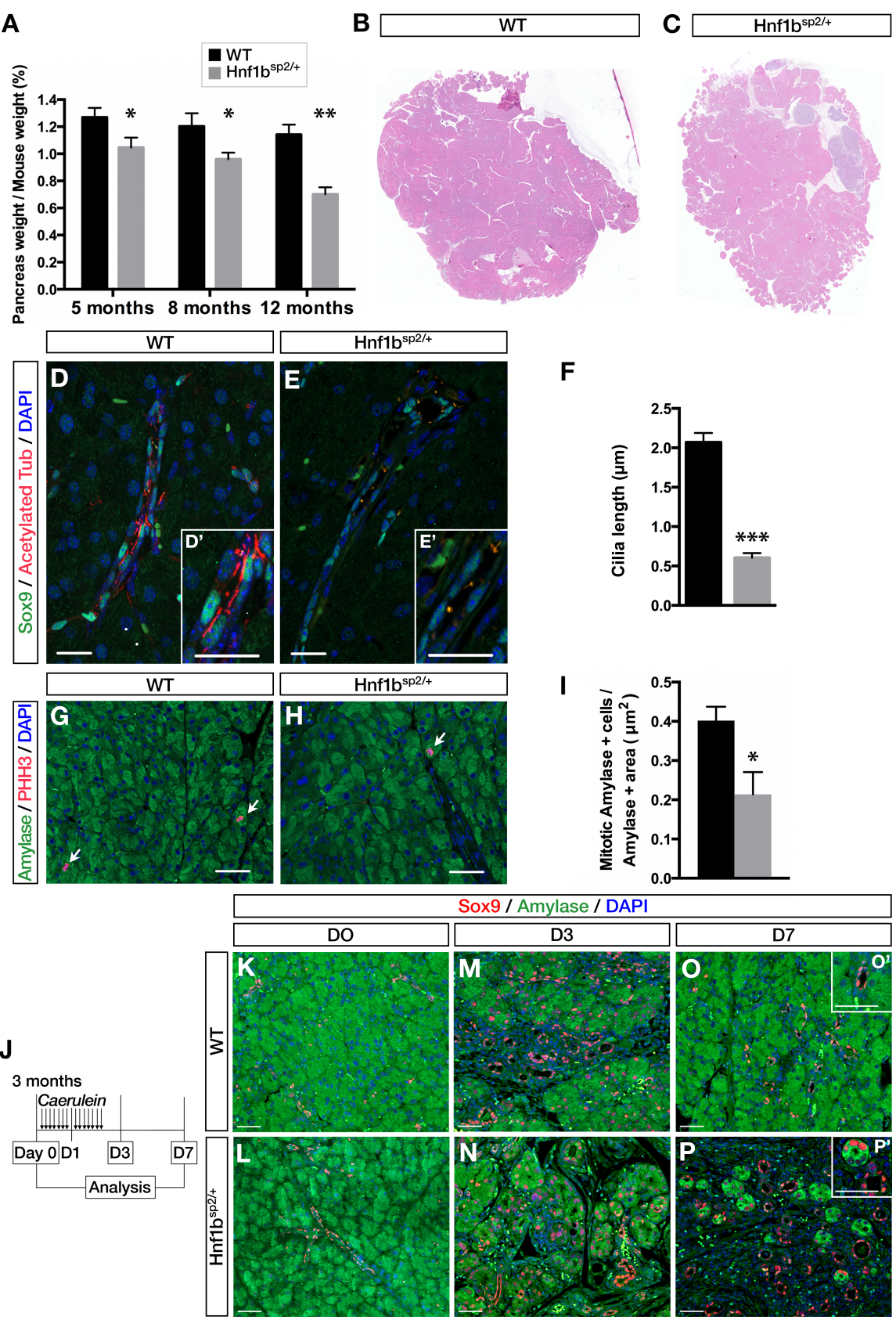

Figure 6 Legend on next page.

Hnf1b[sp2/+] mice develop chronic pancreatitis caused by ductal cell primary cilia defect

Pancreatic hypoplasia and pancreatic exocrine insufficiency constitute a common feature for carriers of *HNF1B* mutations [14,16,20]. *Hnf1b*[sp2/+] mice developed a pancreatic hypoplasia and chronic pancreatitis, with immune infiltration, ADM, loss of acinar cells, fibrosis, and lipomatosis. This was associated with upregulation of *Tgfb1*, increased expression of fibrotic factors, and *Ccn* gene expression. This phenotype increased with age. The primary abnormality of the exocrine phenotype concerned pancreatic ducts, with a dramatic decrease in the length of primary cilia. Ductal cells harbor an immotile primary cilium, functioning as a chemo- and mechano-sensor [83,84], and defective primary cilia result in pancreatitis [85]. Conditional ablation of *Hnf1b* perinatally in ducts caused loss of primary cilia and led to chronic pancreatitis [41], due to downregulation of *Hnf1b* target genes involved in the maintenance of primary cilia, such as *Pkhd1* [86–89]. Novel mutations of *PKHD1* have recently been associated with chronic pancreatitis [90]. A non-cell autonomous mechanism was involved, leading to activation of YAP mechanosensor target genes such as *Ctgf* in acinar cells and upregulation of the TGFβ pathway [41]. These genes are also overexpressed in *Hnf1b*[sp2/+] mice. In correlation, we observed decreased proliferation of acinar cells at 3 months. Moreover, acinar recovery from caerulein-induced acute pancreatitis was impaired in *Hnf1b*[sp2/+] mice at this stage, showing that *Hnf1b*[sp2/+] mice are also more sensitive to developing chronic pancreatitis due to impaired regeneration. This suggests that impaired recovery of the pancreas after injury or infections might contribute to differences in exocrine dysfunction between MODY5 patients. Chronic pancreatitis has been shown to predispose to pancreatic cancer [91]. Conditional ablation of *Hnf1b* in ducts perinatally led to neoplasia and enhanced the ability of oncogenic *KRAS* to promote precancerous lesions [41], suggesting that *HNF1B* is a potential tumor suppressor. Downregulation of *HNF1B* has been associated with risk of renal, prostate, ovarian, colorectal [92–96], and recently pancreatic cancer [97–100]. Although we did not observe precancerous lesions in *Hnf1b*[sp2/+] mice, probably because the timing of pancreatitis onset was too late, it might be interesting to investigate the pancreatic cancer risk of MODY5 patients.

Because *Hnf1b* is not expressed in acinar cells, pancreatitis was not expected in MODY5, and it was proposed that exocrine defects might be caused by pancreas hypoplasia. Phenotypes of mice with inactivated *Hnf1b* develop gradually, depending on the extent of decreased *Hnf1b* expression and the timing of when this defect occurs [36,40,41]. *Hnf1b*[sp2/+] mice show that pancreatitis is associated with a defect in pancreatic ductal cell primary cilia. Thus, hypoplasia observed in MODY5 patients could be caused by a decreased level of *HNF1B* in pancreatic progenitors during embryogenesis; and later, the defect caused by the decreased level of *HNF1B* in pancreatic ducts could lead to a secondary loss of acinar cells and chronic pancreatitis associated with hypoplasia. Furthermore, it is excluded that the exocrine phenotype may influence the onset of MODY5 diabetes in *Hnf1b*[sp2/+] mice, as it appears later than the endocrine one, notably with the maintenance of acinar or ductal marker expression at E17.5.

The *Hnf1b*[sp2/+] mouse model highlights pancreatic exocrine defects in MODY5, confirming that exocrine insufficiency should be systematically investigated in MODY5 patients [32]. Diagnosis of exocrine pancreatic dysfunction in individuals with developmental kidney disease of uncertain cause should prompt a request for *HNF1B* genetic testing.

Taken together, these data show that *Hnf1b*[sp2/+] mice are a suitable model for the study of MODY5/HNF1B syndrome and furnish new insights into the etiology and physiopathology of this disease. The level of *Hnf1b* expression appears crucial to moderate the kinetics and the severity of the phenotype. This might explain why there is a high variability among MODY5 patients, a precise dosage of *HNF1B* being required for normal function during early organogenesis and in adults. *Hnf1b*[sp2/+] mice constituting a novel model of MODY5 diabetes and a model of spontaneous chronic pancreatitis represent a convenient tool for molecular studies and for testing new therapeutic strategies.

Figure 6. Defects in ductal cells are associated with impaired acinar cell proliferation and regeneration in young *Hnf1b*[sp2/+] mice. (A, B) Evolution of pancreas weight/mouse body weight of WT (black) and *Hnf1b*[sp2/+] (grey) mice from 5 to 12 months (5 months: WT, *n* = 16; *Hnf1b*[sp2/+] = 15; 8 months: WT, *n* = 4; *Hnf1b*[sp2/+], *n* = 9; 12 months: WT, *n* = 4; *Hnf1b*[sp2/+], *n* = 4). (B, C) Hematoxylin and eosin staining of WT and *Hnf1b*[sp2/+] pancreatic sections from 3-month-old mice. (D, E) Sox9 (green) and acetylated α-tubulin (Acetylated Tub, red) immunofluorescence at 3 months. Scale bars: 10 μm. (F) Quantification of the length of cilia of ductal cells in WT (black, *n* = 3) and *Hnf1b*[sp2/+] (grey, *n* = 3) at 3 months. (G, H) Phospho-histone H3 (PHH3, red) and amylase (green) immunofluorescence. Arrows indicate mitotic amylase+ cells. Scale bars: 50 μm. (I) Quantification of acinar cell proliferation (amylase+ PHH3+/amylase+ cells) in 3-month-old WT (black, *n* = 3) and *Hnf1b*[sp2/+] (grey, *n* = 3) mice. (J) Experimental design. Three-month-old WT and *Hnf1b*[sp2/+] mice were injected with caerulein hourly, seven times a day, for two consecutive days. Pancreases were harvested before caerulein treatment (D0), and 3 days (D3) and 7 days (D7) after the first caerulein injection. (K–P) Amylase (green) and Sox9 (red) immunofluorescence. Scale bars: 50 μm.

Author contributions statement

EQ, MF, CN, TD, ALM, RCP and CH performed experiments. EQ, MF, CN, TD, ALM, RCP, MG, UA and CH analyzed and interpreted the data. SC provided materials. EQ and CH wrote the manuscript. MF, CN, TD, ALM, SC, RCP, MG and UA revised the manuscript. CH designed, supervised the study and obtained funding.

References

1. Fajans SS, Conn JW. Tolbutamide-induced improvement in carbohydrate tolerance of young people with mild diabetes mellitus. *Diabetes* 1960; **9:** 83–88.

2. Tattersall RB, Fajans SS. A difference between the inheritance of classical juvenile-onset and maturity-onset type diabetes of young people. *Diabetes* 1975; **24:** 44–53.

3. Kleinberger JW, Pollin TI. Undiagnosed MODY: time for action. *Curr Diab Rep* 2015; **15:** 110.

4. Pihoker C, Gilliam LK, Ellard S, *et al.* Prevalence, characteristics and clinical diagnosis of maturity onset diabetes of the young due to mutations in HNF1A, HNF4A, and glucokinase: results from the SEARCH for diabetes in youth. *J Clin Endocrinol Metab* 2013; **98:** 4055–4062.

5. Shields BM, Hicks S, Shepherd MH, *et al.* Maturity-onset diabetes of the young (MODY): how many cases are we missing? *Diabetologia* 2010; **53:** 2504–2508.

6. Thanabalasingham G, Pal A, Selwood MP, *et al.* Systematic assessment of etiology in adults with a clinical diagnosis of young-onset type 2 diabetes is a successful strategy for identifying maturity-onset diabetes of the young. *Diabetes Care* 2012; **35:** 1206–1212.

7. Anik A, Catli G, Abaci A, *et al.* Maturity-onset diabetes of the young (MODY): an update. *J Pediatr Endocrinol Metab* 2015; **28:** 251–263.

8. Fajans SS, Bell GI. MODY: history, genetics, pathophysiology, and clinical decision making. *Diabetes Care* 2011; **34:** 1878–1884.

9. Bellanné-Chantelot C, Clauin S, Chauveau D, *et al.* Large genomic rearrangements in the hepatocyte nuclear factor-1β (*TCF2*) gene are the most frequent cause of maturity-onset diabetes of the young type 5. *Diabetes* 2005; **54:** 3126–3132.

10. Edghill EL, Oram RA, Owens M, *et al.* Hepatocyte nuclear factor-1β gene deletions – a common cause of renal disease. *Nephrol Dial Transplant* 2008; **23:** 627–635.

11. Roehlen N, Hilger H, Stock F, *et al.* 17q12 deletion syndrome as a rare cause for diabetes mellitus type MODY5. *J Clin Endocrinol Metab* 2018; **103:** 3601–3610.

12. Horikawa Y, Iwasaki N, Hara M, *et al.* Mutation in hepatocyte nuclear factor-1 beta gene (TCF2) associated with MODY [letter]. *Nat Genet* 1997; **17:** 384–385.

13. Barbacci E, Chalkiadaki A, Masdeu C, *et al.* HNF1β/TCF2 mutations impair transactivation potential through altered co-regulator recruitment. *Hum Mol Genet* 2004; **13:** 3139–3149.

14. Chen YZ, Gao Q, Zhao XZ, *et al.* Systematic review of TCF2 anomalies in renal cysts and diabetes syndrome/maturity onset diabetes of the young type 5. *Chin Med J (Engl)* 2010; **123:** 3326–3333.

15. Clissold RL, Hamilton AJ, Hattersley AT, *et al.* HNF1B-associated renal and extra-renal disease – an expanding clinical spectrum. *Nat Rev Nephrol* 2015; **11:** 102–112.

16. Dubois-Laforgue D, Cornu E, Saint-Martin C, *et al.* Diabetes, associated clinical spectrum, long-term prognosis, and genotype/phenotype correlations in 201 adult patients with hepatocyte nuclear factor 1B (HNF1B) molecular defects. *Diabetes Care* 2017; **40:** 1436–1443.

17. Alvelos MI, Rodrigues M, Lobo L, *et al.* A novel mutation of the *HNF1B* gene associated with hypoplastic glomerulocystic kidney disease and neonatal renal failure: a case report and mutation update. *Medicine (Baltimore)* 2015; **94:** e469.

18. Ulinski T, Lescure S, Beaufils S, *et al.* Renal phenotypes related to hepatocyte nuclear factor-1β (*TCF2*) mutations in a pediatric cohort. *J Am Soc Nephrol* 2006; **17:** 497–503.

19. Edghill EL, Bingham C, Ellard S, *et al.* Mutations in hepatocyte nuclear factor-1β and their related phenotypes. *J Med Genet* 2006; **43:** 84–90.

20. Bellanné-Chantelot C, Chauveau D, Gautier J, *et al.* Clinical spectrum associated with hepatocyte nuclear factor-1β mutations. *Ann Intern Med* 2004; **140:** 510–517.

21. Nagano C, Morisada N, Nozu K, *et al.* Clinical characteristics of HNF1B-related disorders in a Japanese population. *Clin Exp Nephrol* 2019; **23:** 1119–1129.

22. Bingham C, Hattersley AT. Renal cysts and diabetes syndrome resulting from mutations in hepatocyte nuclear factor-1β. *Nephrol Dial Transplant* 2004; **19:** 2703–2708.

23. Decramer S, Parant O, Beaufils S, *et al.* Anomalies of the *TCF2* gene are the main cause of fetal bilateral hyperechogenic kidneys. *J Am Soc Nephrol* 2007; **18:** 923–933.

24. Faguer S, Decramer S, Chassaing N, *et al.* Diagnosis, management, and prognosis of HNF1B nephropathy in adulthood. *Kidney Int* 2011; **80:** 768–776.

25. Heidet L, Decramer S, Pawtowski A, *et al.* Spectrum of *HNF1B* mutations in a large cohort of patients who harbor renal diseases. *Clin J Am Soc Nephrol* 2010; **5:** 1079–1090.

26. Edghill EL, Bingham C, Slingerland AS, *et al.* Hepatocyte nuclear factor-1 beta mutations cause neonatal diabetes and intrauterine growth retardation: support for a critical role of HNF-1β in human pancreatic development. *Diabet Med* 2006; **23:** 1301–1306.

27. Bingham C, Ellard S, Allen L, *et al.* Abnormal nephron development associated with a frameshift mutation in the transcription factor hepatocyte nuclear factor-1β. *Kidney Int* 2000; **57:** 898–907.

28. Furuta H, Furuta M, Sanke T, *et al.* Nonsense and missense mutations in the human hepatocyte nuclear factor-1β gene (*TCF2*) and their relation to type 2 diabetes in Japanese. *J Clin Endocrinol Metab* 2002; **87:** 3859–3863.

29. Lindner TH, Njolstad PR, Horikawa Y, *et al*. A novel syndrome of diabetes mellitus, renal dysfunction and genital malformation associated with a partial deletion of the pseudo-POU domain of hepatocyte nuclear factor-1β. *Hum Mol Genet* 1999; **8:** 2001–2008.

30. Haldorsen IS, Vesterhus M, Raeder H, *et al*. Lack of pancreatic body and tail in *HNF1B* mutation carriers. *Diabetic Med* 2008; **25:** 782–787.

31. Tjora E, Wathle G, Erchinger F, *et al*. Exocrine pancreatic function in hepatocyte nuclear factor 1β-maturity-onset diabetes of the young (HNF1B-MODY) is only moderately reduced: compensatory hypersecretion from a hypoplastic pancreas. *Diabetic Med* 2013; **30:** 946–955.

32. Clissold RL, Fulford J, Hudson M, *et al*. Exocrine pancreatic dysfunction is common in hepatocyte nuclear factor 1β-associated renal disease and can be symptomatic. *Clin Kidney J* 2018; **11:** 453–458.

33. Iwasaki N, Ogata M, Tomonaga O, *et al*. Liver and kidney function in Japanese patients with maturity-onset diabetes of the young. *Diabetes Care* 1998; **21:** 2144–2148.

34. Bingham C, Ellard S, Cole TR, *et al*. Solitary functioning kidney and diverse genital tract malformations associated with hepatocyte nuclear factor-1β mutations. *Kidney Int* 2002; **61:** 1243–1251.

35. Haumaitre C, Fabre M, Cormier S, *et al*. Severe pancreas hypoplasia and multicystic renal dysplasia in two human fetuses carrying novel *HNF1β/MODY5* mutations. *Hum Mol Genet* 2006; **15:** 2363–2375.

36. Haumaitre C, Barbacci E, Jenny M, *et al*. Lack of TCF2/vHNF1 in mice leads to pancreas agenesis. *Proc Natl Acad Sci U S A* 2005; **102:** 1490–1495.

37. Maestro MA, Boj S, Luco RF, *et al*. *Hnf6* and *Tcf2* (MODY5) are linked in a gene network operating in a precursor cell domain of the embryonic pancreas. *Hum Mol Genet* 2003; **12:** 3307–3314.

38. Nammo T, Yamagata K, Tanaka T, *et al*. Expression of HNF-4alpha (MODY1), HNF-1beta (MODY5), and HNF-1alpha (MODY3) proteins in the developing mouse pancreas. *Gene Expr Patterns* 2008; **8:** 96–106.

39. Solar M, Cardalda C, Houbracken I, *et al*. Pancreatic exocrine duct cells give rise to insulin-producing beta cells during embryogenesis but not after birth. *Dev Cell* 2009; **17:** 849–860.

40. De Vas MG, Kopp JL, Heliot C, *et al*. Hnf1b controls pancreas morphogenesis and the generation of Ngn3$^+$ endocrine progenitors. *Development* 2015; **142:** 871–882.

41. Quilichini E, Fabre M, Dirami T, *et al*. Pancreatic ductal deletion of Hnf1b disrupts exocrine homeostasis, leads to pancreatitis, and facilitates tumorigenesis. *Cell Mol Gastroenterol Hepatol* 2019; **8:** 487–511.

42. Kornfeld JW, Baitzel C, Konner AC, *et al*. Obesity-induced overexpression of miR-802 impairs glucose metabolism through silencing of *Hnf1b*. *Nature* 2013; **494:** 111–115.

43. Bingham C, Ellard S, van't Hoff WG, *et al*. Atypical familial juvenile hyperuricemic nephropathy associated with a hepatocyte nuclear factor-1β gene mutation. *Kidney Int* 2003; **63:** 1645–1651.

44. Harries LW, Ellard S, Jones RW, *et al*. Abnormal splicing of hepatocyte nuclear factor-1 beta in the renal cysts and diabetes syndrome. *Diabetologia* 2004; **47:** 937–942.

45. Thomas CP, Erlandson JC, Edghill EL, *et al*. A genetic syndrome of chronic renal failure with multiple renal cysts and early onset diabetes. *Kidney Int* 2008; **74:** 1094–1099.

46. Kopp JL, Dubois CL, Schaffer AE, *et al*. Sox9$^+$ ductal cells are multipotent progenitors throughout development but do not produce new endocrine cells in the normal or injured adult pancreas. *Development* 2011; **138:** 653–665.

47. Li D-S, Yuan Y-H, Tu H-J, *et al*. A protocol for islet isolation from mouse pancreas. *Nat Protoc* 2009; **4:** 1649–1652.

48. Alanentalo T, Asayesh A, Morrison H, *et al*. Tomographic molecular imaging and 3D quantification within adult mouse organs. *Nat Methods* 2007; **4:** 31–33.

49. Eriksson AU, Svensson C, Hörnblad A, *et al*. Near infrared optical projection tomography for assessments of beta-cell mass distribution in diabetes research. *J Vis Exp* 2013; (71): e50238.

50. Hörnblad A, Nord C, Parween S, *et al*. The pancreas. In *Kaufman's Atlas of Mouse Development Supplement*, Baldock R, Kaufman M, Bard J, *et al*. (eds). Amsterdam, Netherlands: Elsevier, 2016; Ch 6; 85–94.

51. Hörnblad A, Eriksson AU, Sock E, *et al*. Impaired spleen formation perturbs morphogenesis of the gastric lobe of the pancreas. *PLoS One* 2011; **6:** e21753.

52. Cheddad A, Svensson C, Sharpe J, *et al*. Image processing assisted algorithms for optical projection tomography. *IEEE Trans Med Imaging* 2012; **31:** 1–15.

53. Sharpe J, Ahlgren U, Perry P, *et al*. Optical projection tomography as a tool for 3D microscopy and gene expression studies. *Science* 2002; **296:** 541–545.

54. Charrier A, Brigstock DR. Regulation of pancreatic function by connective tissue growth factor (CTGF, CCN2). *Cytokine Growth Factor Rev* 2013; **24:** 59–68.

55. Duan J, Wainwright MS, Comeron JM, *et al*. Synonymous mutations in the human *dopamine receptor D2* (*DRD2*) affect mRNA stability and synthesis of the receptor. *Hum Mol Genet* 2003; **12:** 205–216.

56. Anczuków O, Ware MD, Buisson M, *et al*. Does the nonsense-mediated mRNA decay mechanism prevent the synthesis of truncated BRCA1, CHK2, and p53 proteins? *Hum Mutat* 2008; **29:** 65–73.

57. Pearson ER, Badman MK, Lockwood CR, *et al*. Contrasting diabetes phenotypes associated with hepatocyte nuclear factor-1α and -1β mutations. *Diabetes Care* 2004; **27:** 1102–1107.

58. Brackenridge A, Pearson ER, Shojaee-Moradie F, *et al*. Contrasting insulin sensitivity of endogenous glucose production rate in subjects with hepatocyte nuclear factor-1β and -1α mutations. *Diabetes* 2006; **55:** 405–411.

59. Wang L, Coffinier C, Thomas MK, *et al*. Selective deletion of the *Hnf1β* (MODY5) gene in β-cells leads to altered gene expression and defective insulin release. *Endocrinology* 2004; **145:** 3941–3949.

60. Lee J-Y, Ristow M, Lin X, *et al*. RIP-Cre revisited, evidence for impairments of pancreatic β-cell function. *J Biol Chem* 2006; **281:** 2649–2653.

61. Gu G, Dubauskaite J, Melton DA. Direct evidence for the pancreatic lineage: NGN3+ cells are islet progenitors and are distinct from duct progenitors. *Development* 2002; **129:** 2447–2457.

62. Mellitzer G, Martin M, Sidhoum-Jenny M, *et al*. Pancreatic islet progenitor cells in neurogenin 3-yellow fluorescent protein knock-add-on mice. *Mol Endocrinol* 2004; **18:** 2765–2776.

63. Gradwohl G, Dierich A, LeMeur M, *et al*. Neurogenin3 is required for the development of the four endocrine cell lineages of the pancreas. *Proc Natl Acad Sci U S A* 2000; **97:** 1607–1611.

64. Wang S, Hecksher-Sorensen J, Xu Y, *et al*. Myt1 and Ngn3 form a feed-forward expression loop to promote endocrine islet cell differentiation. *Dev Biol* 2008; **317:** 531–540.

65. Sheets TP, Park KE, Park CH, *et al*. Targeted mutation of *NGN3* gene disrupts pancreatic endocrine cell development in pigs. *Sci Rep* 2018; **8:** 3582.

66. Wang S, Yan J, Anderson DA, *et al*. *Neurog3* gene dosage regulates allocation of endocrine and exocrine cell fates in the developing mouse pancreas. *Dev Biol* 2010; **339:** 26–37.

67. Stanger BZ, Tanaka AJ, Melton DA. Organ size is limited by the number of embryonic progenitor cells in the pancreas but not the liver. *Nature* 2007; **445:** 886–891.

68. Rubio-Cabezas O, Jensen JN, Hodgson MI, *et al*. Permanent neonatal diabetes and enteric anendocrinosis associated with biallelic mutations in *NEUROG3*. *Diabetes* 2011; **60:** 1349–1353.

69. Solorzano-Vargas RS, Bjerknes M, Wang J, *et al*. Null mutations of *NEUROG3* are associated with delayed-onset diabetes mellitus. *JCI Insight* 2020; **5:** e127657.

70. Weir GC, Gaglia J, Bonner-Weir S. Inadequate beta-cell mass is essential for the pathogenesis of type 2 diabetes. *Lancet Diabetes Endocrinol* 2020; **8:** 249–256.

71. Chen C, Cohrs CM, Stertmann J, *et al*. Human beta cell mass and function in diabetes: recent advances in knowledge and technologies to understand disease pathogenesis. *Mol Metab* 2017; **6:** 943–957.

72. Cho J-H, Kim J-W, Shin J-A, *et al*. Beta-cell mass in people with type 2 diabetes. *J Diabetes Invest* 2011; **2:** 6–17.

73. Klinke DJ 2nd. Age-corrected beta cell mass following onset of type 1 diabetes mellitus correlates with plasma C-peptide in humans. *PLoS One* 2011; **6:** e26873.

74. Leete P, Willcox A, Krogvold L, *et al*. Differential insulitic profiles determine the extent of beta-cell destruction and the age at onset of type 1 diabetes. *Diabetes* 2016; **65:** 1362–1369.

75. Henquin JC, Ibrahim MM, Rahier J. Insulin, glucagon and somato-statin stores in the pancreas of subjects with type-2 diabetes and their lean and obese non-diabetic controls. *Sci Rep* 2017; **7:** 11015.

76. Rahier J, Guiot Y, Goebbels RM, *et al*. Pancreatic beta-cell mass in European subjects with type 2 diabetes. *Diabetes Obes Metab* 2008; **10**(suppl 4)): 32–42.

77. Saito K, Yaginuma N, Takahashi T. Differential volumetry of A, B and D cells in the pancreatic islets of diabetic and nondiabetic subjects. *Tohoku J Exp Med* 1979; **129:** 273–283.

78. Sakuraba H, Mizukami H, Yagihashi N, *et al*. Reduced beta-cell mass and expression of oxidative stress-related DNA damage in the islet of Japanese type II diabetic patients. *Diabetologia* 2002; **45:** 85–96.

79. Westermark P, Wilander E. The influence of amyloid deposits on the islet volume in maturity onset diabetes mellitus. *Diabetologia* 1978; **15:** 417–421.

80. Deng S, Vatamaniuk M, Huang X, *et al*. Structural and functional abnormalities in the islets isolated from type 2 diabetic subjects. *Diabetes* 2004; **53:** 624–632.

81. Jo J, Hara M, Ahlgren U, *et al*. Mathematical models of pancreatic islet size distributions. *Islets* 2012; **4:** 10–19.

82. Kilimnik G, Zhao B, Jo J, *et al*. Altered islet composition and dispro-portionate loss of large islets in patients with type 2 diabetes. *PLoS One* 2011; **6:** e27445.

83. Cano DA, Murcia NS, Pazour GJ, *et al*. orpk mouse model of poly-cystic kidney disease reveals essential role of primary cilia in pancre-atic tissue organization. *Development* 2004; **131:** 3457–3467.

84. Lodh S, O'Hare EA, Zaghloul NA. Primary cilia in pancreatic devel-opment and disease. *Birth Defects Res Part C* 2014; **102:** 139–158.

85. Cano DA, Sekine S, Hebrok M. Primary cilia deletion in pancreatic epi-thelial cells results in cyst formation and pancreatitis. *Gastroenterology* 2006; **131:** 1856–1869.

86. Mai W, Chen D, Ding T, *et al*. Inhibition of *Pkhd1* impairs tubulo-morphogenesis of cultured IMCD cells. *Mol Biol Cell* 2005; **16:** 4398–4409.

87. Masyuk TV, Huang BQ, Ward CJ, *et al*. Defects in cholangiocyte fibrocystin expression and ciliary structure in the PCK rat. *Gastroenterology* 2003; **125:** 1303–1310.

88. Menezes LF, Cai Y, Nagasawa Y, *et al*. Polyductin, the *PKHD1* gene product, comprises isoforms expressed in plasma membrane, primary cilium, and cytoplasm. *Kidney Int* 2004; **66:** 1345–1355.

89. Wang S, Luo Y, Wilson PD, *et al*. The autosomal recessive polycys-tic kidney disease protein is localized to primary cilia, with concen-tration in the basal body area. *J Am Soc Nephrol* 2004; **15:** 592–602.

90. Dong F, Chen QQ, Zhuang ZH, *et al*. Multiple gene mutations in patients with type 2 autoimmune pancreatitis and its clinical features. *Cent Eur J Immunol* 2014; **39:** 77–82.

91. Pinho AV, Chantrill L, Rooman I. Chronic pancreatitis: a path to pancreatic cancer. *Cancer Lett* 2014; **345:** 203–209.

92. Buchner A, Castro M, Hennig A, *et al*. Downregulation of HNF-1B in renal cell carcinoma is associated with tumor progression and poor prognosis. *Urology* 2010; **76:** 507.e6–507.e11.

93. Cuff J, Salari K, Clarke N, *et al*. Integrative bioinformatics links HNF1B with clear cell carcinoma and tumor-associated thrombosis. *PLoS One* 2013; **8:** e74562.

94. Grisanzio C, Werner L, Takeda D, *et al*. Genetic and functional ana-lyses implicate the *NUDT11*, *HNF1B*, and *SLC22A3* genes in pros-tate cancer pathogenesis. *Proc Natl Acad Sci U S A* 2012; **109:** 11252–11257.

95. Silva TD, Vidigal VM, Felipe AV, *et al*. DNA methylation as an epi-genetic biomarker in colorectal cancer. *Oncol Lett* 2013; **6:** 1687–1692.

96. Terasawa K, Toyota M, Sagae S, *et al*. Epigenetic inactivation of TCF2 in ovarian cancer and various cancer cell lines. *Br J Cancer* 2006; **94:** 914–921.

97. Hoskins JW, Jia J, Flandez M, *et al*. Transcriptome analysis of pan-creatic cancer reveals a tumor suppressor function for HNF1A. *Carcinogenesis* 2014; **35:** 2670–2678.

98. Janky R, Binda MM, Allemeersch J, *et al*. Prognostic relevance of molecular subtypes and master regulators in pancreatic ductal adeno-carcinoma. *BMC Cancer* 2016; **16:** 632.

99. Klein AP, Wolpin BM, Risch HA, *et al*. Genome-wide meta-analysis identifies five new susceptibility loci for pancreatic cancer. *Nat Commun* 2018; **9:** 556.

100. Li D, Duell EJ, Yu K, *et al*. Pathway analysis of genome-wide asso-ciation study data highlights pancreatic development genes as sus-ceptibility factors for pancreatic cancer. *Carcinogenesis* 2012; **33:** 1384–1390.

SUPPLEMENTARY MATERIAL ONLINE

Figure S1. Growth of WT and *Hnf1b*$^{sp2/+}$ mice

Figure S2. Characterization of abnormal spliced *Hnf1b* transcripts in *Hnf1b*$^{sp2/+}$ pancreases

Table S1. Antibodies

Table S2. Primers used for RT-qPCR

Movie S1. OPT movie of WT pancreas – dorsal lobe

Movie S2. OPT movie of WT pancreas – gastric lobe

Movie S3. OPT movie of WT pancreas – splenic lobe

Movie S4. OPT movie of *Hnf1b*$^{sp2/+}$ pancreas – dorsal lobe

Movie S5. OPT movie of *Hnf1b*$^{sp2/+}$ pancreas – gastric lobe

Movie S6. OPT movie of *Hnf1b*$^{sp2/+}$ pancreas – splenic lobe